The Astronomical Journal, 126:1472–1482, 2003 September

SPECTROSCOPIC STUDY OF Q CYGNI: SURPRISES FROM AN OLD NOVA

S. Kafka,[1] C. Tappert,[2] R. K. Honeycutt,[1] and A. Bianchini[3]
Received 2003 April 23; accepted 2003 May 15

ABSTRACT

We present a time-resolved spectroscopic study of Q Cyg (Nova Cyg 1876), determining a period of $P = 10.08$ hr for the system. Our data also reveal P Cygni profiles in the He I $\lambda\lambda$5876 and 7065 lines and occasionally in the Hα line. Although P Cygni profiles commonly appear in the UV resonance lines of nova-like cataclysmic variables, only BZ Cam was previously known to exhibit a rapidly variable wind, which leaves its signature in time-resolved optical spectral lines. A comparison between BZ Cam and Q Cyg reveals striking similarities between the two systems. The origin of the outflow in Q Cyg and a possible correlation of the P Cygni profiles with the system's optical state are discussed.

Key words: binaries: close — novae, cataclysmic variables — stars: fundamental parameters — stars: individual (Q Cygni)

1. INTRODUCTION

Although Q Cyg (Nova Cyg 1876) is one of the oldest novae known, the parent cataclysmic variable (CV) is poorly studied. Known to be a very fast nova, it reached visual magnitude 3 for about 4 days before declining (Shara, Potter, & Shara 1989). The few published photometric observations of the object have revealed long-term quasi-periodic variations of about 0.6 mag (Shugarov 1983; Shara et al. 1989), which are likely to be the same features that Honeycutt, Robertson, & Turner (1998) have called stunted outbursts, having a typical recurrence interval of 1–2 months. Like most old nova and novalike CVs, Q Cyg has Balmer lines in emission (Shara et al. 1986; Downes et al. 1995), but the strengths of Hγ and He I λ5876 were seen to significantly change between two observations spaced by 5 days (Downes et al. 1995). In this paper we present the first time-resolved spectroscopic study of Q Cyg, deriving an orbital period for the system based on radial velocity variations of Hα. Our data also reveal P Cygni profiles in both Hα and helium lines, as well as remarkable changes in He I line strengths and profiles from night to night, indicating that the outflow related to the P Cygni profiles is quite irregular.

In §§ 2 and 3 we describe our observations and in § 4 we discuss our results. In § 5 we discuss the red/near-IR spectral features of the system and their changing line strengths and profiles, whereas in § 6 we summarize our conclusions.

2. SPECTROSCOPIC OBSERVATIONS AND REDUCTIONS

Two sets of spectroscopic data were used in this study, incorporating observations from the Asiago Observatory at Cima Ekar[4] and from the WIYN Observatory.[5]

The system was first observed in 2000 July and August, using the AFOSC[6] system, attached to the 1.82 m telescope of the Asiago Observatory. One spectrum was obtained with the blue (4450–6660 Å) grism 7 (resolution 9 Å), whereas for the time-resolved spectroscopy we used the red (6330–8175 Å) grism 8 (resolution 7 Å), giving a resolution of 4 pixels in both cases. No photometric or flux standards were observed. Table 1 contains a log of the observations. Data reduction was performed using IRAF routines (Tody 1993). Bias and dome flat frames were used to correct for the CCD characteristics, whereas one-dimensional spectra were obtained using the optimal extraction algorithm (Horne 1986). The spectra were calibrated in wavelength with respect to helium (grism 7) and thorium (grism 8) lamps, yielding typical residuals of 1.4 Å or 0.8 pixels. For further analysis of the Asiago spectroscopic data, we used the ESO-MIDAS software (Warmels 1992).

The WIYN data were acquired during parts of four successive nights in the summer of 2002, using the blue cable of the HYDRA multiobject spectrograph on the WIYN 3.5 m telescope at Kitt Peak, under good weather and seeing conditions. The 600 line mm^{-1} grating was used in first order, blazed at 7500 Å; the spectral coverage was ~5300–8000 Å, with a resolution of ~3.5 Å. Exposure times were 600 s. Dome flats were obtained on all four nights, sky subtraction was performed using information from numerous unparked fibers, and a CuAr lamp was used for wavelength calibration. An observing log is included in Table 1. Reduction of the data was conducted using the IRAF/NOAO packages. The steps included extraction of one-dimensional star and sky fiber spectra, flat-field correction, wavelength calibration, correction for scattered light, sky subtraction, and removal of the continuum. No corrections were made for atmospheric extinction; therefore, telluric absorption features remain in the final WIYN spectra.

3. PHOTOMETRIC OBSERVATIONS AND REDUCTIONS

Simultaneous photometric data were taken during both Asiago runs using a V filter; a summary of the observations is presented in Table 1. Reductions were made using the

[1] Department of Astronomy, Indiana University, 319 Swain Hall West, Bloomington, IN 47405.
[2] Departamento de Física, Grupo de Astronomía, Universidad de Concepción, Casilla 160-C, Concepción, Chile.
[3] Dipartimento di Astronomia, Università di Padova, Vicolo dell'Osservatorio 2, I-35122 Padova, Italy.
[4] The telescope and its instruments are operated by the Astronomical Observatory of Padua, which is part of the Instituto Nazionale di Astrofisica (INAF), Italy.
[5] The WIYN Observatory is a joint facility of the University of Wisconsin-Madison, Indiana University, Yale University, and the National Optical Astronomy Observatory (NOAO).
[6] Asiago Faint Object Spectrograph and Camera.

TABLE 1
OBSERVING LOG OF Q CYGNI

Date (UT)	Telescope	Grism/Fiber/Filter	*N* Observations	Exposure (s)
		Spectroscopic Observations		
2000 Jul 28	Asiago	7	1	1800
	Asiago	8	10	600
2000 Jul 30	Asiago	8	13	600
2000 Aug 23	Asiago	8	20	600
2000 Aug 24	Asiago	8	27	600
2000 Aug 25	Asiago	8	22	600
2002 Jun 17	WIYN	Blue	15	600
2002 Jun 18	WIYN	Blue	16	600
2002 Jun 19	WIYN	Blue	14	600
2002 Jun 20	WIYN	Blue	17	600
		Photometric Observations		
2000 Jul 27	Asiago	*V*	119	30
2000 Jul 28	Asiago	*V*	4	30
2000 Jul 30	Asiago	*V*	4	30
2000 Aug 23	Asiago	*V*	5	30
2000 Aug 24	Asiago	*V*	5	30
2000 Aug 25	Asiago	*V*	6	30

IRAF/DAOPHOT package and the stand-alone DAOMATCH and DAOMASTER routines (Stetson 1992). Differential magnitudes for Q Cyg were computed with respect to five known nonvariable field stars. Comparison with the list of secondary photometric standards in the field of Q Cyg by Henden & Honeycutt (1997) showed 22 coinciding objects; three of the comparison stars used for our magnitude calibrations were among them. Calibration for the remaining 19 common stars yielded an uncertainty of 0.03 mag for the zero point of the calibrated photometry.

An automated 0.41 m telescope in Indiana[7] acquired photometric data near the times of the spectroscopic runs. The data were reduced using the method of incomplete ensemble photometry (Honeycutt 1992) employing 150 comparison stars. This data forms an extension to the earlier RoboScope photometry of Q Cyg presented in Honeycutt et al. (1998). Six secondary standards from Henden & Honeycutt (1997) were used to fix the zero point with an accuracy of 0.01 mag. The average error of the Indiana Q Cyg photometry is 0.02 mag.

4. RESULTS

4.1. *Photometry*

Figure 1 presents a close-up of the light curve for Q Cyg obtained during the Asiago run, showing variations of $\sim$0.1 mag on timescales of $\sim$25 minutes. This could be due to either flickering or other quasi-periodic variations, but longer data sets would be needed to make a distinction between these two effects. In either case, the variations are indicative of the presence of an accretion disk. The general characteristics of the Asiago data sets are summarized in Table 2. Columns (2) and (3) give the faint and bright magnitudes for each night; the errors correspond to the photometric uncertainty for each data point. In column (4) the average magnitudes of the sets are listed, with the error corresponding to the standard deviation of the averaging process.

Figure 2 shows three seasons of Q Cyg photometry that encompass the three spectroscopic runs (marked). The data is particularly rich near the time of the Asiago spectroscopy when photometry from both the Asiago telescope and RoboScope are available. For most of the intervals shown in Figure 2, Q Cyg is seen to continue the stunted outburst-like behavior described in Honeycutt et al. (1998). From the top panel, it is obvious that at the time of the first Asiago spectroscopic run Q Cyg was in a relatively faint state, while spectra of the second Asiago run were obtained at the peak of a stunted outburst or quasi-periodic oscillation of the system. The 2002 WIYN spectra (Fig. 2, *bottom*) were obtained on the rising branch of a well-defined local maximum in brightness. Finally, there is no indication of eclipses in the long-term Q Cyg photometry from RoboScope.

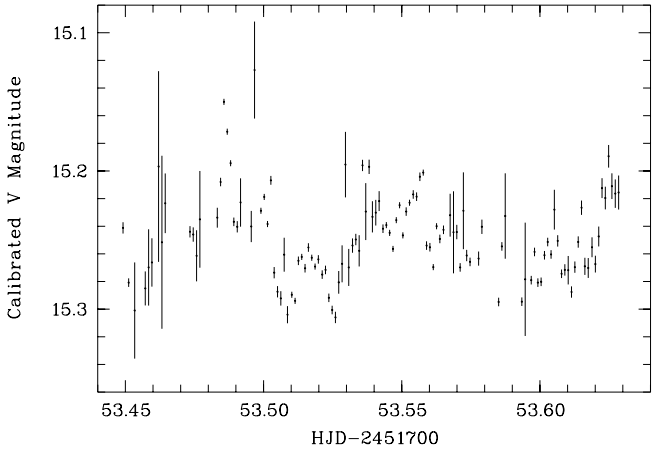

FIG. 1.—Light curve of Q Cyg over 4.3 hr on 2000 July 27 (UT)

[7] RoboScope; Honeycutt & Turner 1992.

TABLE 2
CHARACTERISTICS OF THE ASIAGO DATA SETS

Date (UT) (1)	V_{min} (mag) (2)	V_{max} (mag) (3)	V_{av} (mag) (4)
2002 Jul 27	15.306(07)	15.127(36)	15.249(34)
2000 Jul 28	15.317(06)	15.285(06)	15.304(14)
2000 Jul 30	15.346(07)	15.212(06)	15.292(59)
2000 Aug 23	14.630(06)	14.538(06)	14.574(35)
2000 Aug 24	14.602(06)	14.559(06)	14.583(17)
2000 Aug 25	14.754(06)	14.636(06)	14.705(49)

4.2. *Spectroscopy*

Figure 3 contains the single blue Asiago spectrum, whereas Figures 4 and 5 display average individual spectra for each night with prominent spectral features identified.

Fits were made for the strength and velocity of the Hα line in order to study their time dependence. For the Asiago data a single Gaussian was fitted to the line profile and the radial velocity was computed with respect to the atmospheric absorption near 7600 Å in order to minimize effects due to uncertainties in the wavelength calibration and to air-mass variations. The radial velocities were subsequently corrected for Earth's motion relative to the local standard of rest. For the WIYN data, a single Voigt profile was fitted to the Hα line and heliocentric radial velocities were calculated.

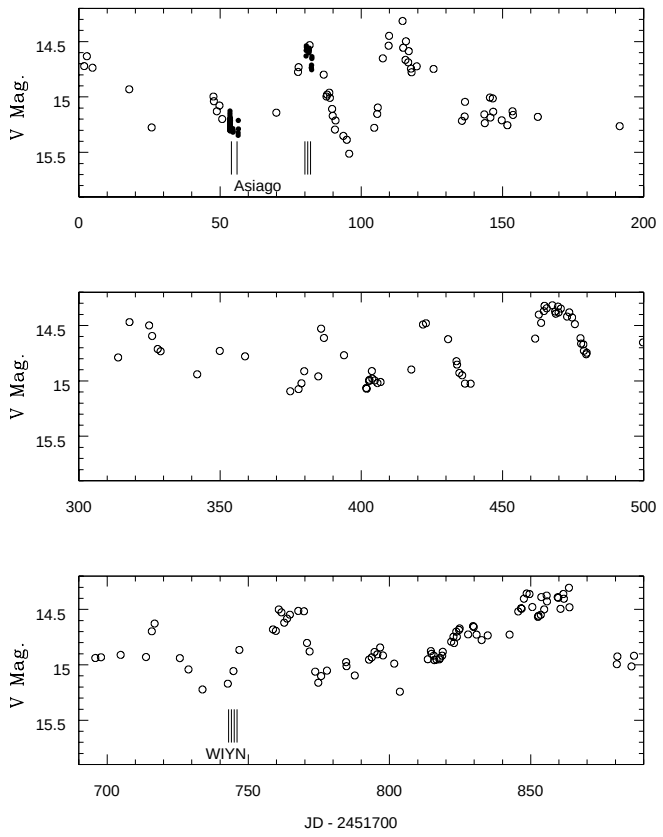

FIG. 2.—RoboScope light curve of Q Cyg (*open circles*), including the Asiago photometric data from the 2000 July and August runs (*filled circles*). The dates of our spectroscopic observations are marked in the top and bottom panels of the graph.

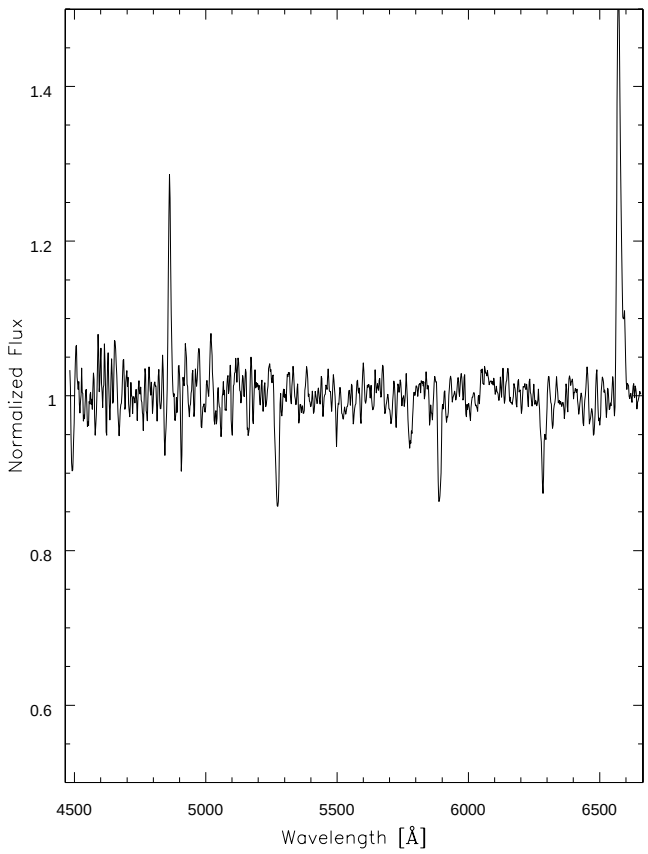

FIG. 3.—Asiago blue spectrum from 2000 July 28 (UT) with the continuum normalized to unity. A 3 pixel averaging filter has been applied to smooth the data without loss of information.

Extensive periodogram and period-folding analyses of the radial velocities were performed on the Asiago and WIYN data in various combinations. Using all of the data for the determination of the period is ineffective because of cycle count ambiguities between the Asiago and WIYN epochs. Since the two Asiago runs are separated by 4 weeks, the Asiago data set has considerably more leverage on the period than the WIYN data set. Figure 6 contains a periodogram of the Asiago data. The analysis-of-variance (AOV) algorithm (Schwarzenberg-Czerny 1989) as implemented in MIDAS was used to investigate the Asiago data set for periodic variations. The highest peak and the stronger secondary peaks due to aliases (corresponding to the 4 week separation of the two Asiago runs) are presented in Table 3. The most probable one of these is

$$P_2 = 0.4202(3) \text{ days} = 10.085(6) \text{ hr} .$$

The errors were computed with a Monte Carlo method (Mennickent & Tappert 2001). When folding the radial velocities v_r with this period and fitting a sinusoidal function

$$v_r(\varphi) = \gamma - K_1 \sin(2\pi\varphi) , \quad (1)$$

one notices an offset of $\sim$50 km s^{-1} in the constant term γ for the 2000 August 24 data set. An artificial effect appears unlikely, since all radial velocities have been computed with respect to the same telluric line. The 2000 July 30 data might be affected in a similar way (the residuals are close to those of the August 24 data), but the 2000 July set as a whole

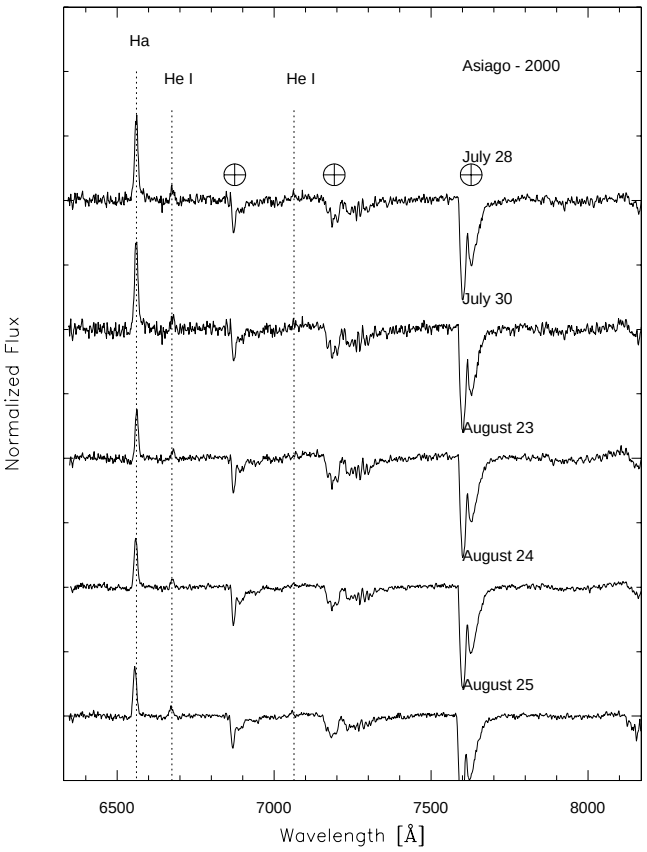

FIG. 4.—Averaged red Asiago data for each night of our observations. The vertical axis is normalized flux with respect to the continuum. A shift was applied for display purposes and the most prominent lines are identified.

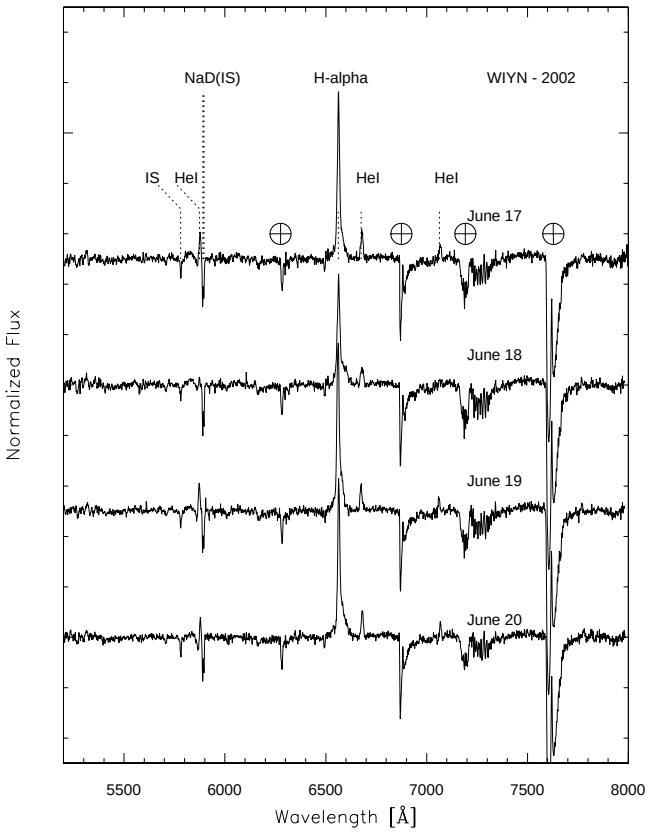

FIG. 5.—Same as Fig. 4, but for the WIYN data

consists of too few data points for a confirmation. Adjusting both the July 30 and the August 24 data sets for $\gamma = 50$ km s^{-1} increases the power of all peaks considerably, especially for P_2 and P_3, with P_2 still being the highest. In Table 3, the brackets in the second column contain the values after the γ correction. The WIYN periodogram, based on four nights of spectroscopic monitoring, shows a strong peak at $P = 0.4148$ days, which is very close to the Asiago period. Folding the WIYN data on the Asiago period leads to the radial velocity plot of Figure 7 (*middle*). No γ corrections were applied to the WIYN data.

Each data set was folded separately on both the highest peak and the primary aliases, confirming that the highest peak of 10.085 hr is the preferred period. This period is adopted to fold both the Asiago and WIYN data onto phase. The zero point for the phasing of the Asiago and WIYN folding was determined separately, to insure that phase zero corresponds to the positive-to-negative crossing of the radial velocities for both epochs, as shown in Figure 7.

Using the phasing given by the radial velocity fit, we display in Figure 8 the phase dependence of the equivalent widths (EW) of the Hα line for each of the three runs. It is clear that only the data of the second Asiago run (*middle*) has a well-defined sinusoidal variation. The data of the first Asiago run (*top*), although having incomplete phase

TABLE 3
FREQUENCIES FROM THE AOV PERIODOGRAM

f (cycles day^{-1})	Power	P (days)	P (hr)	Peak
2.342(2).....	42.3(60.5)	0.4271(3)	10.250(8)	P_1
2.380(2).....	53.5(86.4)	0.4202(3)	10.085(6)	P_2
2.418(2).....	49.8(75.3)	0.4136(3)	9.927(7)	P_3
2.456(2).....	40.5(53.4)	0.4072(3)	9.772(8)	P_4

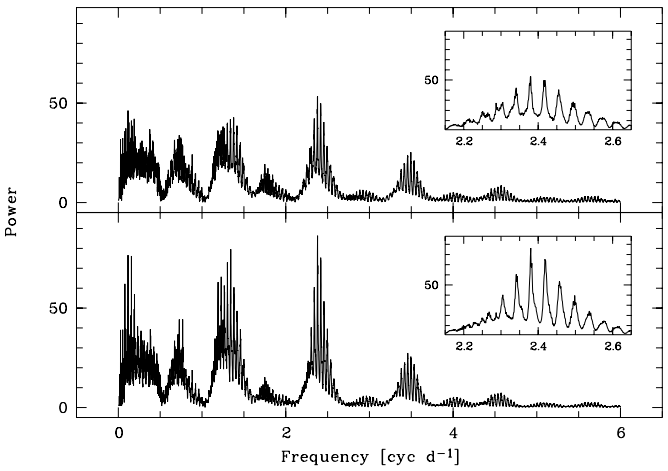

FIG. 6.—*Top*: AOV periodogram for the original data set. *Bottom*: Periodogram of the data after correcting for the γ shift in sets from 2000 July 30 and August 24 (see text). The inserts show a close-up of the region around $P = 10$ hr.

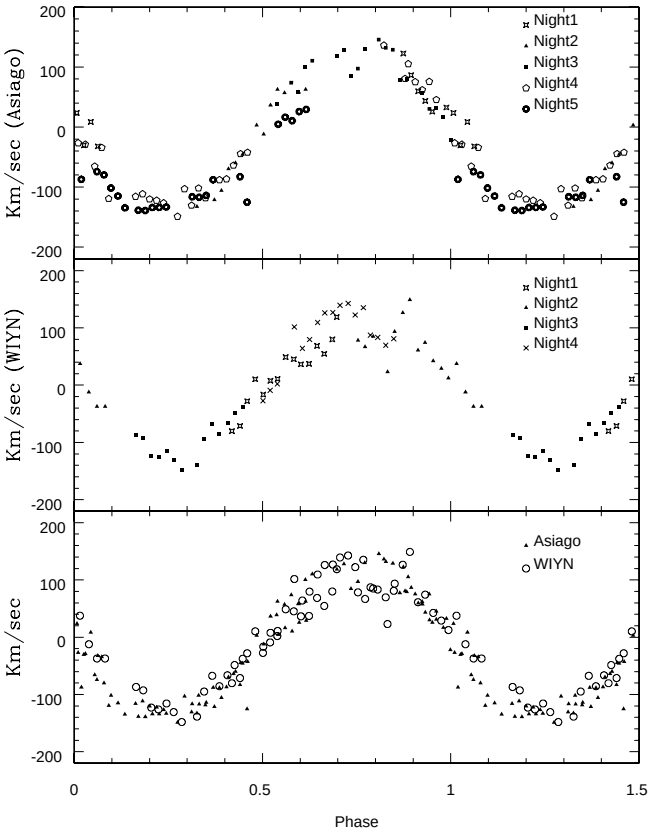

FIG. 7.—Radial velocities folded on $P = 0.4202$ days. Each night of observations is represented by a different symbol in the top and middle panels. For each data set, phase zero corresponds to the positive-to-negative crossing of the secondary star. *Top*, Asiago data; *middle*, WIYN data; *bottom*, Asiago (*triangles*) and WIYN (*circles*) data.

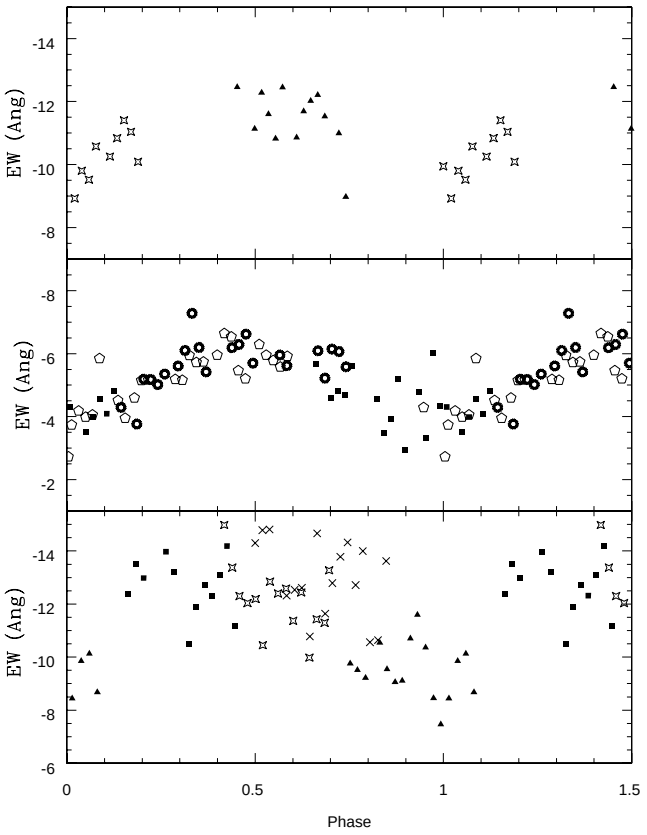

FIG. 8.—Hα emission-line equivalent widths vs. phase for the Asiago runs (*top* and *middle*) and the WIYN run (*bottom*). Different symbols correspond to each of the nights of our observations.

coverage, is consistent with the variation in the middle panel. (Note however that the mean strength of Hα is 2 times weaker in the middle panel, corresponding to an outburst state.) In the WIYN data (*bottom*) a sinusoidal phase variation is present but is not well defined, probably because of an erratic broad emission wing at the red edge of the line, which will be discussed later in the paper. Although we were able to extract a period from our data sets, the 2 yr separation between the Asiago and the WIYN runs is too large to obtain a single accurate ephemeris for the system. Therefore, we provide the radial velocity measurements in Table 4 for future investigation of the period.

5. THE WIND CHARACTERISTICS

The most striking features of the time-resolved spectra of the system (Fig. 9) are prominent absorption components at the blue edges of the He I $\lambda\lambda$5876 and 7067 lines and occasionally at the Hα line, which evolve with time. Those features—known as P Cygni profiles—are characteristic of outflows, winds, or expanding shells surrounding a system. In CVs, they are commonly observed in the UV resonance lines of novalike systems (in species such as C IV λ1549, Si IV λ1397, and N IV λ1240; Drew 1997) or in the Balmer lines of novae right after the maximum of the explosion, indicating either axisymmetric (V382 Velorum 1999; Shore et al. 2003), asymmetric (Nova Centauri 1995; Yan Tse et al. 2001), or spherical expansion of the ejecta. However, on a handful of occasions, P Cygni profiles have been reported to occur at the optical subordinate lines of novalike systems undergoing outburst, like in AT Cnc (Smith et al. 1997; Nogami et al. 1999) and TW Vir (Smith et al. 1997).

The P Cygni lines are undoubtedly formed via scattering of continuum photons in an expanding bipolar wind arising from an accretion disk (e.g., Shlosman & Vitello 1993); however, the mechanism for driving the wind remains uncertain. The most widely discussed driving mechanisms are resonance scattering of photons from the hot inner accretion disk or boundary layer (e.g., Proga, Stone, & Drew 1998) and/or magneto-centrifugal forces originating in the cooler outer portions of the disk face (Cannizzo & Pudritz 1988). In all cases, winds appear to be observed most often in systems with high mass transfer rates ($\dot{M}$), i.e., high-luminosity disks.

Q Cyg is the second CV in which time-resolved spectroscopy in the optical reveals evolving wind features in the form of emission lines with P Cygni profiles. The first is BZ Cam, which is also the only CV that it is located at the apex of a bow-shaped nebula. It is thought that the wind from BZ Cam interacts with the ambient interstellar gas to produce a bow shock (Hollis et al. 1992), but alternative origins for the nebula have also been discussed (Griffith, Fabian, & Sion 1995; Greiner et al. 2001). The strong BZ Cam wind produces optical P Cygni profiles, whose time dependence has been investigated by Ringwald & Naylor (1998, hereafter RN) to deduce properties of the wind. Although the BZ Cam and Q Cyg data have differing spectral and time resolutions, $\sim$1.5 Å (our estimate) versus 3.3 Å

TABLE 4
Q Cygni Radial Velocities

JD − 2,451,700	v_r (km s^{-1})	JD − 2,451,700	v_r (km s^{-1})	JD − 2,451,700	v_r (km s^{-1})	JD − 2,451,700	v_r (km s^{-1})
54.513	122.6	81.471	−28.9	56.450	3.2	742.961	79.9
54.522	86.5	81.482	−65.5	81.463	−26.7	742.966	118.8
54.530	59.6	81.490	−34.4	81.471	−28.9	743.83	78.4
54.538	43.6	81.497	−119.3	81.482	−65.5	743.838	66.8
54.546	25.8	81.527	−115.6	81.490	−34.4	743.847	85.1
54.561	32.7	81.535	−111.5	81.497	−119.3	743.863	23.0
54.569	23.6	81.543	−120.2	81.527	−115.6	743.871	93.5
54.577	−30.4	81.551	−122.4	81.535	−111.5	743.880	126.5
54.585	8.5	81.559	−126.5	81.543	−120.2	743.888	149.0
54.592	−32.2	81.574	−148.9	81.551	−122.4	743.897	61.2
56.384	−132.6	81.582	−103.2	81.559	−126.5	743.905	74.3
56.403	−121.2	81.59	−130.6	81.574	−148.9	743.914	42.4
56.411	−105.7	81.598	−101.8	81.582	−103.2	743.923	29.0
56.419	−69.6	81.605	−118.2	81.59	−130.6	743.931	12.6
56.427	−59.9	81.621	−88.1	81.598	−101.8	743.940	37.6
56.435	−45.8	81.629	−86.7	81.605	−118.2	743.950	−12.2
56.450	3.2	81.637	−63.9	81.621	−88.1	743.959	−37.2
56.458	−11.9	81.644	−44.7	81.629	−86.7	743.968	−37.2
56.466	36.5	81.652	−42.4	81.637	−63.9	744.843	−86.8
56.474	62.6	82.307	−87.1	81.644	−44.7	744.851	−92.7
56.482	57.1	82.325	−74.3	81.652	−42.4	744.860	−122.8
56.497	58.1	82.332	−79.8	82.307	−87.1	744.868	−126.1
56.505	62.6	82.340	−101.7	82.325	−74.3	744.877	−115.7
80.424	39.0	82.348	−114.9	82.332	−79.8	744.885	−130.7
80.440	73.7	82.356	−134.6	82.340	−101.7	744.894	−148.0
80.448	58.7	82.371	−138.7	82.348	−114.9	744.911	−138.6
80.456	100.3	82.379	−139.1	82.356	−134.6	744.919	−95.0
80.464	110.3	82.386	−134.1	82.371	−138.7	744.928	−67.4
80.491	118.6	82.394	−134.0	82.379	−139.1	744.936	−85.5
80.499	127.8	82.402	−133.1	82.386	−134.1	744.945	−66.5
80.507	84.8	82.431	−116.2	82.394	−134.0	744.953	−48.6
80.515	97.2	82.439	−117.1	82.402	−133.1	744.962	−37.7
80.523	130.1	82.447	−113.9	82.431	−116.2	745.825	−27.4
80.538	145.6	82.454	−87.8	82.439	−117.1	745.833	−9.0
80.546	131.9	82.484	−82.7	82.447	−113.9	745.841	2.1
80.554	128.8	82.492	−125.2	82.454	−87.8	745.860	101.7
80.562	77.6	82.527	4.6	82.484	−82.7	745.869	64.1
80.569	79.5	82.535	16.5	82.492	−125.2	745.877	79.6
80.587	57.6	82.543	10.6	742.849	−80.3	745.886	109.5
80.595	30.1	82.550	25.7	742.858	−71.3	745.894	126.1
80.602	31.1	82.558	29.4	742.866	−28.0	745.903	126.9
80.610	16.9	54.569	23.6	742.875	10.3	745.911	139.3
80.618	−22.0	54.577	−30.4	742.884	−16.5	745.920	142.7
81.384	136.3	54.585	8.5	742.892	7.8	745.928	122.4
81.408	80.6	54.592	−32.2	742.900	10.9	745.937	135.2
81.411	105.3	56.384	−132.6	742.909	48.8	745.945	87.15
81.419	75.2	56.403	−121.2	742.918	45.2	745.953	83.2
81.427	61.9	56.411	−105.7	742.926	36.5	745.962	69.7
81.435	75.7	56.419	−69.6	742.935	37.2	745.971	81.1
81.443	45.5	56.427	−59.9	742.944	68.6		
81.463	−26.7	56.435	−45.8	742.952	54.6		

and 1 minute versus 10 minutes for the two data sets, respectively, a comparison between them reveals interesting similarities and distinctions.

The variable character of the Q Cyg spectrum was first noted by Downes et al. (1995), in which features like the He I λ5876 emission line appear to be absent in one of the two reported spectra, spaced by 5 days. In the single blue Asiago spectrum (2000 July 28) this same feature (He I λ5876 emission) is also missing. In the WIYN night-to-night average spectra, this feature is present during nights 1, 3, and 4, but it is absent in night 2 (2002 June 18). In addition, in the WIYN spectra, strong P Cygni profiles, which are variable in strength and erratic in appearance, are evolving at the blue edge of this He I line. For BZ Cam, the P Cygni profile of the He I λ5876 line is the most sensitive wind indicator and its irregular character indicates a variable outflow from the system. In Q Cyg, in addition to the fluctuating nature of the He I λ5876 line, resembling that of BZ Cam, P Cygni profiles are occasionally seen at the He I λ7065 line during the times when the P Cygni profiles are strongest at 5876 Å.

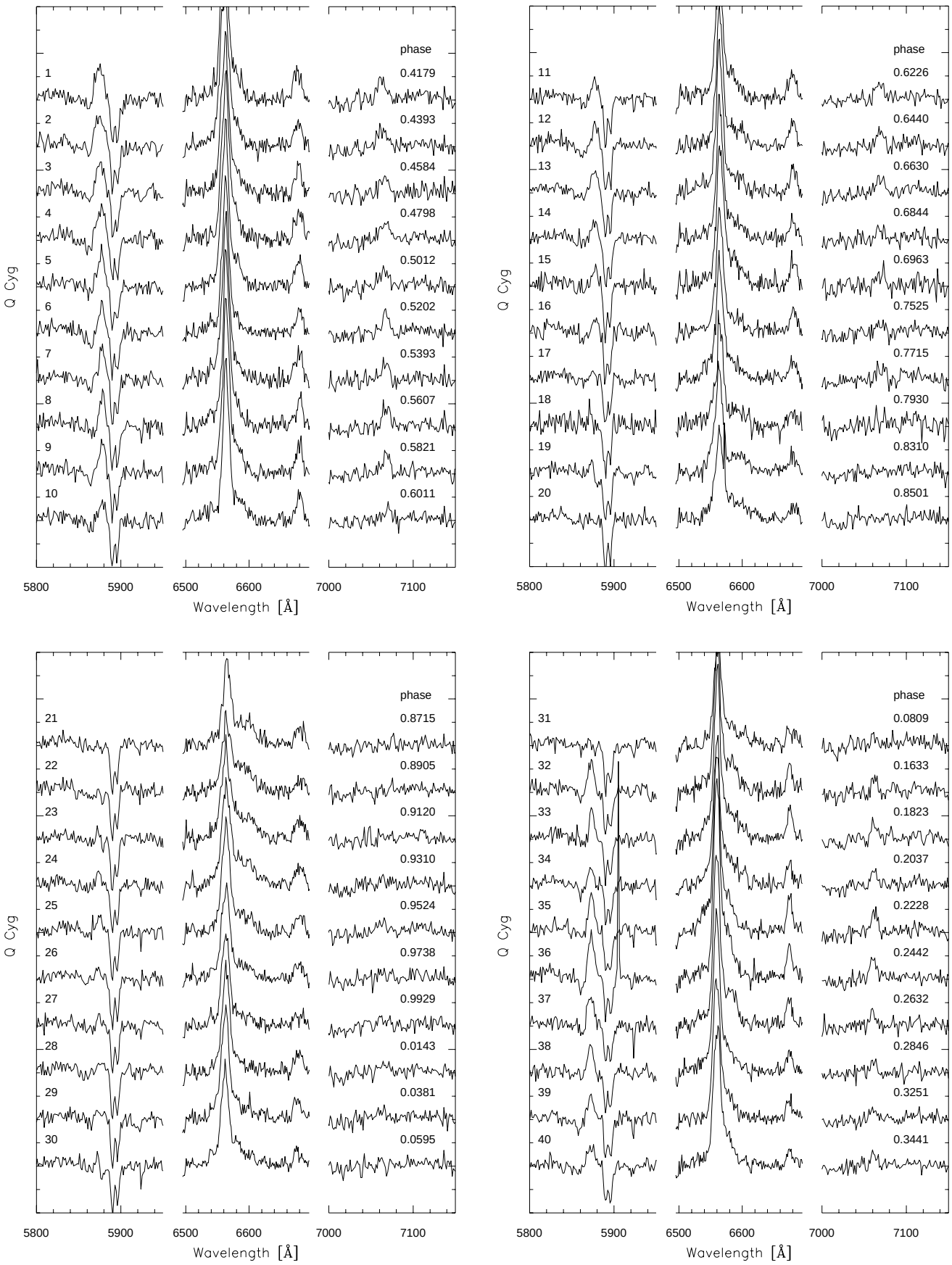

FIG. 9.—Time sequence of the WIYN spectra, expanded over three spectral regions that contain the strongest emission lines. Spectra 1–16 correspond to night 1, spectra 17–31 to night 2, spectra 32–45 to night 3, and spectra 46–62 to night 4. A dashed vertical line has been added at the absorption component of He I λ5876 for the event of night 4 (spectra 47–54), in order to demonstrate that the wind velocity decreases as the event progresses.

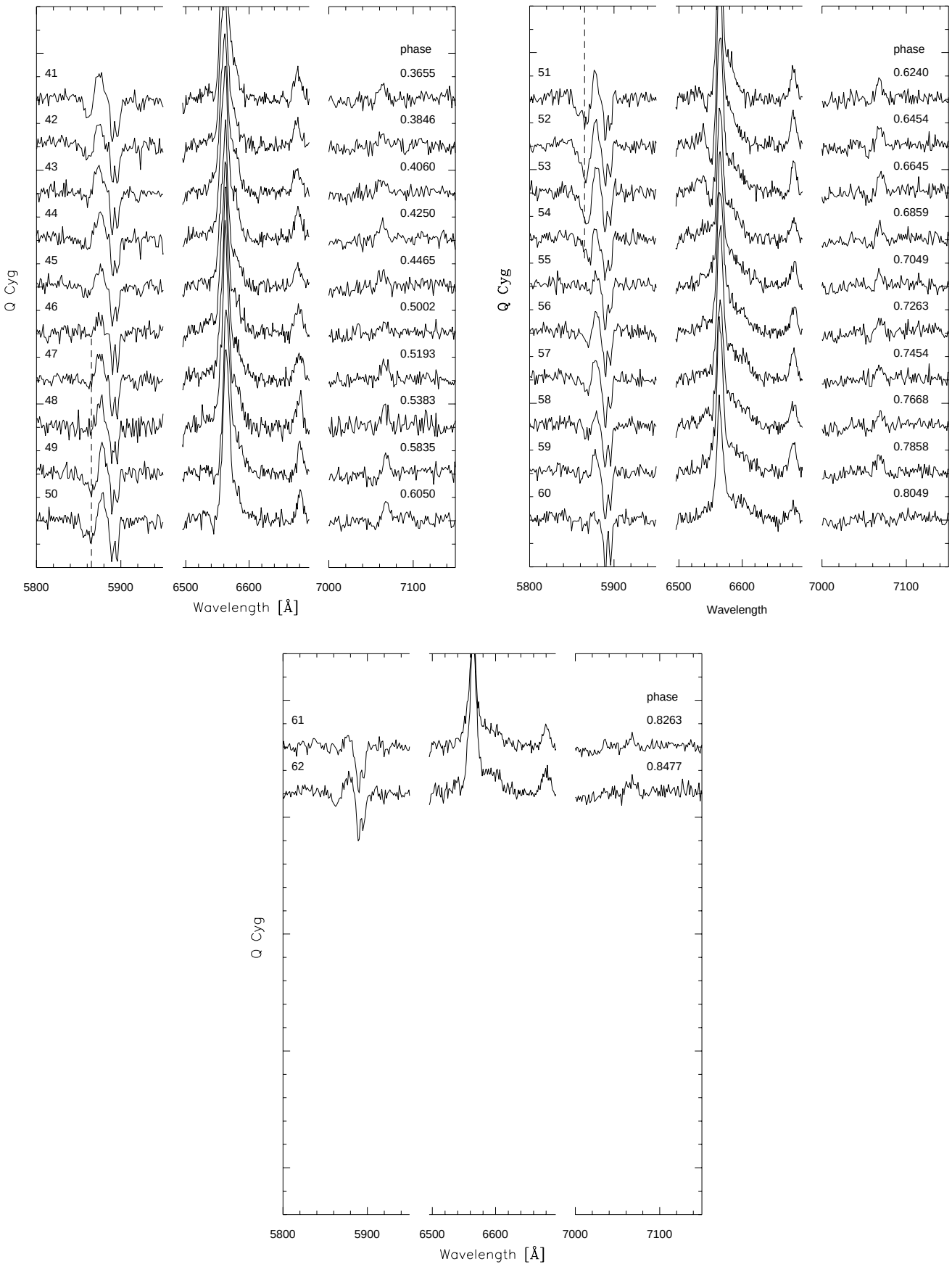

FIG. 9.—*Continued*

The He I λ7065 line, although weak, is present in all the Asiago data. Unfortunately, RN's BZ Cam data do not extend red enough to allow a comparison of the behavior of this line for the two systems. Surprisingly enough, the He I λ6678 line does not have any absorption component in either Q Cyg or BZ Cam.

RN found the BZ Cam wind to be present about half the time during two nights in 1995, in discrete events lasting 30–40 minutes. In our 2002 Q Cyg spectra in Figure 9, blue-shifted absorption appears in He I λ5876 about one-third of the time; however, the wind events in Q Cyg seem to have a variety of more complex behaviors: on night 1 (Fig. 9) the wind features are weak but often present, whereas on night 2 they are mostly absent. On night 3 the wind was erratic, changing over one or two 10 minute exposures. The 3.5 hr of spectra from night 4 are characterized by a well-defined wind episode with a total duration of about 1.5 hr. Overall, the wind events in Q Cyg appear to last longer than those in BZ Cam and are somewhat more erratic.

RN's time sampling of the BZ Cam spectra allows the detection of discrete evolving events in the wind of that system, with wind variations occuring as rapidly as every 6–8 minutes. Although our spectra are characterized by less frequent time sampling, we can interpret the Q Cyg outflow to be of stochastic (as opposed to discrete) nature. Therefore, although a red emission wing, variable in strength, appears to be present in the Hα line in all the WIYN spectra, indicating a receding outflow, a P Cygni profile at this line appears only during night 4, coinciding with a deeper absorption feature at the blue end of both the He I $\lambda\lambda$5876 and 7065 lines, indicating an enhanced wind event. Similar behavior appears in the Hα line of BZ Cam. There is some evidence of a P Cygni profile in the August Asiago data; however, the lower resolution and the red spectral range (which does not include the most-affected He I λ5876 line) compromise an unambiguous detection.

In BZ Cam the terminal velocities of the wind are $\sim$3000 km s^{-1}. Unlike the winds in OB stars, the BZ Cam velocities are seen to decline with time during the wind event (RN). The most blueward absorption in Q Cyg is $\sim$1500 km s^{-1}, for both Hα and He I λ5876. During the most well-defined wind event that we observed in Q Cyg (from night 4), the central velocity of the absorption component declines with time, as can be seen in Figure 9 (spectra 49–58). Based on BZ Cam and Q Cyg, one may tentatively expect that a wind velocity that declines with time during a wind enhancement event is a property common to CV winds.

In addition, Griffith et al. (1995) find evidence for a phase dependence of the P Cyg character of the UV resonance lines in BZ Cam. RN find no correlation with orbital phase for the optical wind lines in BZ Cam, but their phase coverage was uneven, thus no firm conclusion was drawn. The same situation holds for the WIYN Q Cyg data—we see no obvious phase dependence, but we have overlapping coverage only for phases $\sim$0.5–0.7 (nights 1 and 4).

5.1. *The* He I *Lines*

The two He I lines that sometimes have P Cygni profiles ($\lambda\lambda$5876 and 7065) result from transitions in the He I triplet system, whose populations are affected by the strong metastable effective ground state 2 ^3S; the individual line transitions are 2 $^3P \rightarrow 3\ ^3S$ and 2 $^3P \rightarrow 3\ ^3D$, respectively. More than three decades ago, Robbins (1968) argued that collisional transitions are very effective in depopulating the 2 ^3P level, applied in nebulae of average and above average density. These effects are due to the strong metastability of the 2 ^3S level, which becomes overpopulated in conditions of low density and dilute radiation fields. Absorption and reprocessing of photons from 2 ^3S alter the recombination cascade and overpopulate 2 ^3P, making absorption in He I $\lambda\lambda$5876 and 7065 more probable under low-density conditions (Robbins 1968; Almong & Netzer 1989; Proga, Mikolajewska, & Kenyon 1994; Benjamin, Skillman, & Smits 2002). On the other hand, this is not the case for He I λ6678 (2 $^1P \rightarrow 3\ ^1D$), part of a singlet system without strong metastable levels. Although it is beyond of the scope of this paper to explore the particular radiative transfer effects responsible for the He I line behavior in Q Cyg, we can infer that the different behaviors of the three helium lines are likely to be traced to the optical depth and density differences of two prominent regions of the system: the disk and the ouflow. The density-sensitive He I $\lambda\lambda$5876 and 7065 lines apparently trace changes in the wind, leading to intensity variations in the sense that those lines are stronger when the wind is weaker. The latter is supported by the fact that the P Cygni profile in the He I λ5876 during night 4 appears to be deeper at the same time that the emission component of the line becomes weaker, indicating an increase in the wind density (also remember that, at that epoch, P Cygni profiles evolve at the Hα wings).

Using the WIYN data alone, we see that He I $\lambda\lambda$5876 and 7067 emission EWs (Fig. 10) follow the same orbital variations as Hα, in contrast to the He I λ6678 line, which seems to be invariant with orbital phase. A model in which the EW

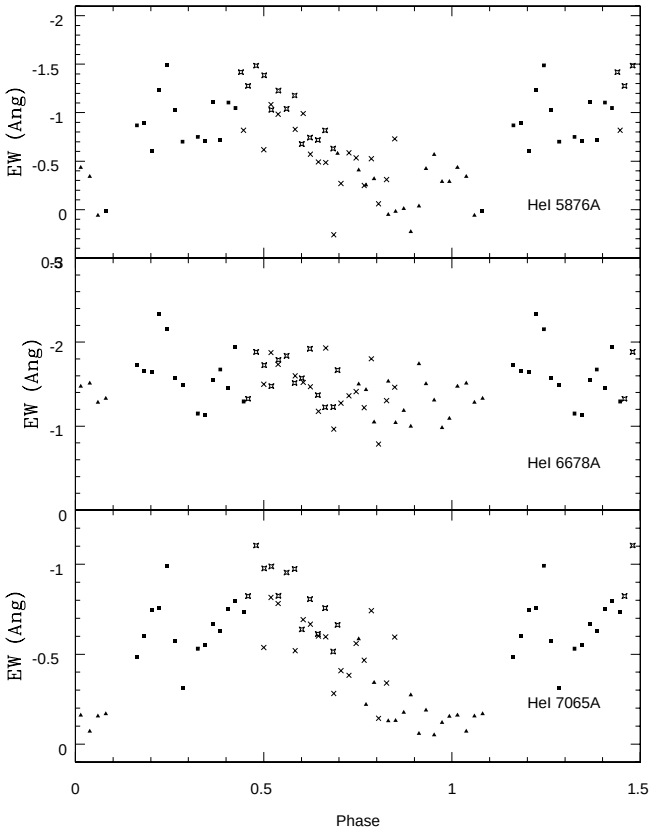

FIG. 10.—Equivalent widths of the three He I lines vs. phase for the WIYN data. Different symbols correspond to different nights.

variation is due to an eclipse of the wind by the secondary star appears reasonable in light of the behavior of He I λ6678 and the fact that most of the emission lines are weakest just at phase zero, i.e., at the part of the orbit where the secondary star is near inferior conjunction. Furthermore, the absence of P Cygni profiles in the He I λ6678 line suggests that it does not originate from the same physical part of the system as the He I λ5876 and He I λ7067 lines. In BZ Cam, the double-peaked nature of the He I λ6678 line suggests that the line originates from the accretion disk (RN). However, our resolution does not allow us to resolve a double-peak in the line profile. A coherent picture of Q Cyg can be formed by assuming that He I λ6678 arises primarily from a relatively thin disk that is uneclipsed by the secondary star in this low inclination system (noneclipsing), whereas the other He I lines arise primarily in a bipolar wind whose vertical extent is such that a significant portion of the wind is eclipsed by the secondary star near phase zero.

Although the spectral resolution of the Asiago data is $\sim$2 times greater than the WIYN spectra, it is likely that wind profiles would have been detected during the 2000 July and August runs if the wind was as active as seen in the 2002 June WIYN data. This raises the question of the long-term presence/variability of the wind, especially since the three spectroscopic runs were obtained at different parts of the 0.5 mag quasi-periodic or stunted outburst photometric variations (Fig. 2) of the system. A recent study of BZ Cam (Greiner et al. 2001), presenting photometric and spectroscopic data during different optical states of the system, revealed that the P Cygni profiles of the Hα line, which were prominent when BZ Cam was in high state, were absent when the system went to its intermediate and low states. At the same time, all the emission lines strengthen with the decreasing of the brightness of the system. It is likely that the appearance/disappearance of the P Cygni profiles is linked to the outburst behavior of the systems, in which case, this should be a global characteristic of winds in CVs.

5.2. *Additional Spectral Characteristics*

The Na D lines (at 5890 and 5896 Å) in Q Cyg are stationary and therefore interstellar in origin. In BZ Cam, RN used the strength of interstellar Na D to estimate the distance and luminosity, finding $3.8 < M_V < 5.3$, which places BZ Cam among the most luminous CVs. We measure the equivalent width of the Na D doublet in the WIYN data of Q Cyg to be 1.65 ± 0.1 Å. Following RN's procedure, we find $d = 3.3$ kpc. Assuming mean $V = 15$ (Fig. 2) and $A_V = 0.8$ (Warner 1995), we find $M_V = 1.6$. Old novae at a period of about 10 hr appear as bright as $M_V = 2.4$ (QZ Aur; Warner 1995). Although the Na D technique is not expected to be very accurate, it appears that Q Cyg is among the most luminous postnovae, which is consistent with the fact that P Cygni wind lines are seen in the optical spectrum of Q Cyg.

Finally, we searched for a signature of the secondary star superimposed on the spectrum of Q Cyg. For long period systems, earlier type secondaries are expected. Nevertheless, we searched for indications of the presence of TiO bands, which would imply that the secondary is a late-K–early-M spectral type star, but found none. Unfortunately, the spectral features expected from a more likely late G-type companion are quite weak in the near-IR spectral regions we have available.

6. CONCLUSIONS

We present a spectroscopic study of the old nova Q Cyg (Nova Cygni 1876). We deduce a period for the system, $P = 10.08$ hr, placing it among the long-period CVs. Our data also reveal the signature of an intermittent outflow (wind) from the system, leaving its signature as evolving P Cygni profiles in the He I $\lambda\lambda$5876 and 7065 lines, and a short-lived absorption feature in the Hα line.

It is not clear whether the 0.5 mag luminosity variations seen in novalike CVs are due to mass transfer variations or to disk instabilities. In either case, an increase in disk luminosity may result in an interval of increased wind activity. The timescale of the wind events in Q Cyg is similar to that of the photometric variations shown in the Asiago data of Figure 1. If the wind events are associated with an increase in disk luminosity, there may well be a photometric signature associated with the appearance of the optical P Cygni profiles. Therefore, it would be quite interesting to obtain an extended run of simultaneous spectroscopy and photometry of Q Cyg, which would reveal the behavior of the spectral lines of the system at different optical states.

The geometry and time dependence of various wind mechanisms can be quite distinct, lending importance to time- and orbit-resolved studies of the line profiles. Therefore, CV outflows provide insight not only into the spatial and kinematic structure of winds, but also into the mechanism for driving the winds, the associated mass loss, and the loss of angular momentum from the system. In Q Cyg, the He I $\lambda\lambda$5876 and 7065 lines most likely emerge from the outflow, whereas the He I λ6678 is a signature of the disk. Striking similarities of the absorption features of Q Cyg with the ones present in BZ Cam (which is known to be embedded in a bow-shock nebula) lead to the belief that winds in CVs may be related to the intermediate/high optical states of the systems. This hypothesis, if confirmed in other CVs, can provide a unique way in which outflows from these systems can be studied in the optical regime using ground-based telescopes, providing significant insight into the mechanism of the different optical states of CVs and the origin of the wind.

We gratefully acknowledge the efforts of G. Turner and B. Adams for helping keep the automated telescope running productively. This research has made use of the SIMBAD database, operated at CDS, Strasbourg, France.

REFERENCES

Almog, Y., & Netzer, H. 1989, MNRAS, 238, 57
Benjamin, R. A., Skillman, E. D., & Smits, D. P. 2002, ApJ, 569, 288
Cannizzo, J. K., & Pudritz, R. E. 1988, ApJ, 327, 840
Downes, R., Hoard, D. W., Szkody, P., & Wachter, S. 1995, AJ, 110, 1824
Drew, J. E. 1997, in IAU Colloq. 163, Accretion Phenomena and Associated Outflows, ed. D. T. Wickramasinghe, L. Ferrario, & G. V. Bicknell (ASP Conf. Ser. 121) (San Francisco: ASP), 465
Greiner, J., et al. 2001, A&A, 376, 1031
Griffith, D., Fabian, D., & Sion, E. M. 1995, PASP, 107, 856
Henden, A. A., & Honeycutt, R. K. 1997, PASP, 109, 441
Hollis, J. M., Oliversen, R. J., Wagner, R. M., & Feibelman, W. A. 1992, ApJ, 393, 217
Honeycutt, R. K. 1992, PASP, 104, 435
Honeycutt, R. K., Robertson, J. W., & Turner, G. W. 1998, AJ, 115, 2527
Honeycutt, R. K., & Turner, G. W. 1992, in ASP Conf. Ser. 34, Robotic Telescopes in the 1990s, ed. A. V. Filippenko (San Francisco: ASP), 77
Horne, K. 1986, PASP, 98, 609
Mennickent, R. E., & Tappert, C. 2001, A&A, 372, 563

Nogami, D., Masuda, S., Kato, T., & Hirata, R. 1999, PASJ, 51, 115
Proga, D., Mikolajewska, J., & Kenyon, S. J. 1994, MNRAS, 268, 213
Proga, D., Stone, J. M., & Drew, J. E. 1998, MNRAS, 295, 595
Ringwald, F. A., & Naylor, T. 1998, AJ, 115, 286
Robbins, R. R. 1968, ApJ, 151, 497
Schwarzenberg-Czerny, A. 1989, MNRAS, 241, 153
Shara, M. M., Livio, M., Moffat, A. F. J., & Orio, M. 1986, ApJ, 311, 163
Shara, M. M., Potter, M., & Shara, D. J. 1989, PASP, 101, 985
Shlosman, I., & Vitello, P. 1993, ApJ, 409, 372
Shore, S. N., et al. 2003, AJ, 125, 1507
Shugarov, S. Y. 1983, Astron. Tsirk., 1252, 6
Smith, R., Sarna, M. J., Catalan, M. S., & Jones, D. H. P. 1997, MNRAS, 287, 271
Stetson, P. B. 1992, in ASP Conf. Ser. 25, Astronomical Data Analysis Software and Systems I, ed. D. M. Worrall, C. Biemesderfer, & J. Barnes (San Francisco: ASP), 291
Tody, D. 1993, in ASP Conf. Ser. 52, Astronomical Data Analysis Software and Systems II, ed. R. J. Hanisch, R. J. V. Brissenden, & J. Barnes (San Francisco: ASP), 173
Warmels, R. H. 1992, in ASP Conf. Ser. 25, Astronomical Data Analysis Software and Systems I, ed. D. M. Worrall, C. Biemesderfer, & J. Barnes (San Francisco: ASP), 115
Warner, B. 1995, Cataclysmic Variable Stars (Cambridge: Cambridge Univ. Press)
Yan Tse, J., Hearnshaw, J. B., Rosenzweig, P., Guzman, E., Escalona, O., Gilmore, A. C., Kilmartin, P. M., & Watson, L. C. 2001, MNRAS, 324, 553